Cellular and Molecular Bioengineering, Vol. 10, No. 5, October 2017 *(© 2017)* pp. 387–403
DOI: 10.1007/s12195-017-0489-4

Phase-Separated Liposomes Enhance the Efficiency of Macromolecular Delivery to the Cellular Cytoplasm

Zachary I. Imam, Laura E. Kenyon, Grant Ashby, Fatema Nagib, Morgan Mendicino, Chi Zhao, Avinash K. Gadok, and Jeanne C. Stachowiak

Department of Biomedical Engineering, The University of Texas at Austin, Austin, TX, USA

(Received 7 February 2017; accepted 11 May 2017; published online 22 May 2017)

Associate Editor Michael R. King oversaw the review of this article.

Abstract

Introduction—From viruses to organelles, fusion of biological membranes is used by diverse biological systems to deliver macromolecules across membrane barriers. Membrane fusion is also a potentially efficient mechanism for the delivery of macromolecular therapeutics to the cellular cytoplasm. However, a key shortcoming of existing fusogenic liposomal systems is that they are inefficient, requiring a high concentration of fusion-promoting lipids in order to cross cellular membrane barriers.

Objectives—Toward addressing this limitation, our experiments explore the extent to which membrane fusion can be amplified by using the process of lipid membrane phase separation to concentrate fusion-promoting lipids within distinct regions of the membrane surface.

Methods—We used confocal fluorescence microscopy to investigate the integration of fusion-promoting lipids into a ternary lipid membrane system that separated into liquid-ordered and liquid-disordered membrane phases. Additionally, we quantified the impact of membrane phase separation on the efficiency with which liposomes transferred lipids and encapsulated macromolecules to cells, using a combination of confocal fluorescence imaging and flow cytometry.

Results—Here we report that concentrating fusion-promoting lipids within phase-separated lipid domains on the surfaces of liposomes significantly increases the efficiency of liposome fusion with model membranes and cells. In particular, membrane phase separation enhanced the delivery of lipids and model macromolecules to the cytoplasm of tumor cells by at least four-fold in comparison to homogenous liposomes.

Conclusions—Our findings demonstrate that phase separation can enhance membrane fusion by locally concentrating fusion-promoting lipids on the surface of liposomes. This work represents the first application of lipid membrane phase separation in the design of biomaterials-based delivery systems. Additionally, these results lay the ground work for developing fusogenic liposomes that are triggered by physical and molecular cues associated with target cells.

Keywords—DOTAP, Fusion, Transmembrane delivery, Membrane, Biophysics, Biomaterials.

Address correspondence to Jeanne C. Stachowiak, Department of Biomedical Engineering, The University of Texas at Austin, Austin, TX, USA. Electronic mail: jcstach@austin.utexas.edu

Jeanne C. Stachowiak, Ph.D Dr. Jeanne Stachowiak completed her undergraduate education in mechanical engineering at the University of Texas at Austin in 2002. She received a master's degree in mechanical engineering from the University of California, Berkeley in 2004, under the supervision of Professor Arun Majumdar and a doctorate in mechanical engineering from the University of California, Berkeley in 2008 under the supervision of Professor Daniel Fletcher. From 2008 to 2011 Dr. Stachowiak served as a Senior Member of the Technical Staff at Sandia National Laboratories, where her independent research program explored basic biophysical questions and practical applications of lipid membrane materials and systems. Dr. Stachowiak has served as a tenure-track Assistant Professor in the Department of Biomedical Engineering at the University of Texas at Austin since January 2012. Through quantitative molecular-scale measurements and the design of biomimetic materials, research in her laboratory aims to understand the physical basis of cellular membrane organization and to design biologically-inspired materials and systems for biomedical applications.

This article is part of the 2017 CMBE Young Innovators special issue.

ABBREVIATIONS

DPPC	1,2-Dipalmitoyl-*sn*-glycero-3-phosphocholine
DOPC	1,2 Dioleoyl-*sn*-glycero-3-phosphocholine
DOTAP	1,2 Dioleoyl–3-trimethylammonium-propane
PEG2000-DPPE	1,2 Dipalmitoyl-*sn*-glycerol-3-phosphoethanolamine-*N*-[Methoxy(Polyethylene glycol)-2000]
Texas Red-DPPE	Texas Red-1,2-dipalmitoyl-*sn*-glycero-3-phosphoethanolamine
Oregon Green-DPPE	Oregon Green-1,2-dipalmitoyl-*sn*-glycero-3-phosphoethanolamine
mol%	Molar fraction
GUV	Giant unilamellar vesicle
SUV	Small unilamellar vesicle
Rhodamine B-dextran	Rhodamine B isothiocyanate-dextran average molecular weight of 10,000
TRITC-dextran	Tetramethylrhodamine isothiocyanate-dextran average molecular weight of 20,000

INTRODUCTION

Fusion of lipid membranes is an essential process used by biological systems in diverse contexts from the release of neurotransmitters during fusion of synaptic vesicles to the cellular plasma membrane[49] to the release of viral DNA and proteins into the cellular cytoplasm during fusion of the viral envelope with the target cell surface.[8] Beyond its natural physiological roles, fusion of synthetic liposomes to cellular membranes offers the possibility of efficient delivery of liposome-encapsulated macromolecules to the cellular interior. In particular, an increasing group of therapeutics including genes, proteins, and other macromolecules lack significant membrane permeability, creating a growing need for novel membrane transport strategies.[13,17,33,39] Toward the goal of harnessing membrane fusion for delivery, enveloped viruses[46,54,59] have been engineered to incorporate genes and other therapeutic macromolecules.[31,41,54] However, risks associated with the use of live viruses have hampered this approach.[3] Similarly, recent reports of the capacity of exosomes and other extracellular vesicles to deliver macromolecules suggest their potential as delivery agents, yet limited understanding of their delivery mechanisms, lack of purity in their preparation, and the difficulty of loading them with specific cargos are challenges that remain to be addressed.[1,4,24,51]

Therefore, despite advancements in biologically derived delivery systems we presently lack a simple and easily controllable system for macromolecular delivery to the cellular interior. Toward realizing this goal, synthetic molecules that promote membrane fusion have been developed, including fusogenic lipids[34,55] and surfactants[16,30] as well as fusogenic peptides.[42,44,58] While these approaches have been demonstrated to drive delivery of diverse macromolecules including whole genes[11,12] and proteins,[27] they require large doses of fusion-promoting molecules, making them inefficient in comparison to biological fusion systems, and often leading to toxicity and immunogenicity *in vivo*.[10,14,28,36]

A potential means of reducing the overall concentration of fusogenic molecules required for macromolecular delivery would be to design liposomal carriers that concentrate fusogenic molecules within small regions of the membrane surface, which could potentially act as a fusogenic "patch" on the liposome surface. This idea is inspired by membrane phase separation, the process by which membranes separate into regions of distinct lipid composition based on the physical and chemical properties of their head groups and hydrocarbon tail groups. Phase separation of biological membranes is a ubiquitous natural mechanism for locally concentrating specific lipid species on membrane surfaces,[23,52,53] which cells harness to organize diverse membrane processes such as viral budding, assembly of the immunological synapse, and even cell–cell fusion events.[8,9,19] Additionally, phase separation has been utilized to enhance targeting in immunoliposomes.[20,21] However, membrane phase separation has not been applied in the design of biomaterials for therapeutic delivery.

Motivated by the ability of membrane phase separation to organize molecular events at membrane surfaces here we investigate the potential of membrane phase separation to locally concentrate fusogenic lipids in order to enhance the efficiency of membrane fusion events and promote the delivery of membrane-impermeable molecules to the cellular cytoplasm. Specifically, we found that the fusogenic lipid, DOTAP (1,2 dioleoyl–3-trimethylammonium-propane), can be combined with cholesterol and the saturated lipid DPPC (1,2-dipalmitoyl-*sn*-glycero-3-phosphocholine) to form a ternary lipid system that spontaneously separates into liquid ordered and liquid disordered phases. By exploring this phase diagram we identified a range of lipid compositions for which DOTAP is tightly concentrated within a minority region on the membrane surface. Further, we found that concentrating DOTAP within such regions substantially en-

hanced the ability of liposomes to transfer lipids to synthetic vesicles and cells, and boosted the transfer of the model hydrophilic macromolecule, dextran, to the cellular cytoplasm. These results suggest a novel path forward for the design of controllable fusogenic membrane materials that can drive efficient macromolecular delivery to the cellular interior.

RESULTS AND DISCUSSION

Membrane Phase Separation can be Used to Concentrate the Fusogenic Lipid DOTAP Within Distinct Regions on Liposome Surfaces

We first set out to determine whether the model fusogenic lipid, DOTAP, could be integrated into a phase-separated lipid system. In particular, we sought a means of creating vesicles that concentrated DOTAP into small, phase-separated regions of the membrane surface, which could be used to promote membrane fusion. Toward this goal we explored the incorporation of DOTAP into a phase separating ternary lipid system. Ternary lipid systems consisting of (i) a lipid with a melting point well below ambient temperature; (ii) a lipid with a melting point well above ambient temperature; and (iii) a sterol, such as cholesterol, have frequently been found to separate into co-existing liquid ordered and liquid disordered phases near room temperature when mixed in appropriate ratios (Fig. 1a).[52] In these systems, lipids with zwitterionic head groups and unsaturated tail groups, such as DOPC (1,2 dioleoyl-*sn*-glycero-3-phosphocholine), which has a melting temperature of −17 °C, have often been chosen as the low temperature melting component. Here we replaced this component with DOTAP, which has a cationic head group that promotes membrane fusion[43] but has the same unsaturated oleoyl tail groups as DOPC, giving it a low melting temperature, <5 °C[45] (Fig. 1a). Additionally, the saturated lipid used in this system, DPPC, has a high melting temperature, 41 °C (Fig. 1a).

We began by mapping the phase diagram of the ternary system DOTAP/DPPC/cholesterol in order to identify compositions for which the system displayed phase separation at room temperature. This effort was guided by the published DOPC/DPPC/cholesterol phase diagram,[52] as well as the spatial distribution of the fluorescent probe lipid, Texas-Red DPPE (Texas Red-1,2-dipalmitoyl-*sn*-glycero-3-phosphoethanolamine), which was included at a trace concentration of 0.3 mol% in all of the compositions we examined. This probe lipid is known to partition toward highly fluid phases and away from liquid ordered and solid phases.[48] To map this ternary system's phase diagram,

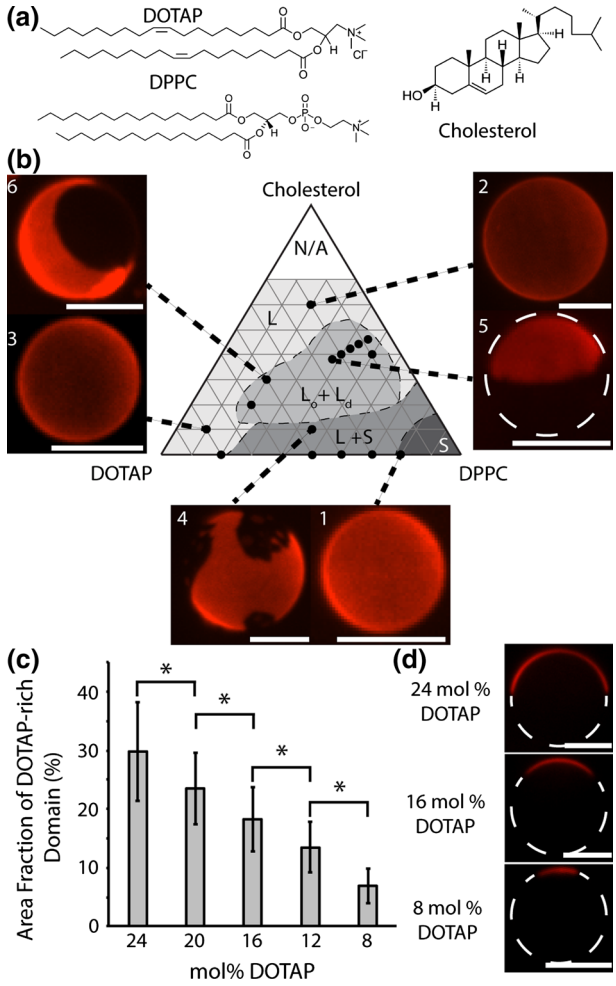

FIGURE 1. DOTAP can be integrated into a phase-separated membrane system. (a) Molecular structure of lipids. DOTAP (Top), DPPC (Bottom), cholesterol (Right). (b) A ternary DOTAP/DPPC/cholesterol phase diagram that plots the phases present at room temperature (25 °C) for multiple mixtures of DOTAP, DPPC, and cholesterol. All data superimposed over the published phase diagram for the DOPC/DPPC/cholesterol system.[52] The phase boundaries of this diagram are marked with dashed lines because the phase regions of the DOTAP/DPPC/cholesterol system are likely not identical to the DOPC/DPPC/cholesterol system owing to the physio-chemical differences between the headgroups of DOTAP and DOPC. Closed circles indicate points where confocal fluorescence microscopy images were taken. A trace amount (0.3 mol%) of Texas Red-DPPE was used to visualize contrast between phases. As discussed in the text, composition 1 displays a uniform solid phase. Compositions 2 and 3 display a single uniform liquid phase. Composition 4 displays liquid–solid phase coexistence. Composition 5 displays liquid–liquid phase coexistence where the liquid ordered phase makes up the majority of the vesicle. Composition 6 displays liquid–liquid phase coexistence where the liquid disordered phase makes up the majority. All scale bars correspond to 5 μm. (c) Bar chart displaying the average fraction of the highly fluid phase as a function of the molar concentration of DOTAP in the mixture. Error bars represent standard deviation. The area fraction of the domain of at least 16 vesicles were measured per data point. Brackets show statistically significant comparisons using an unpaired, 2-tailed student's *t*-test. All p values < 0.003. (d) Confocal fluorescence microscopy slices of phase-separated 24, 16, and 8 mol% DOTAP GUVs, each with a 1:1 ratio of cholesterol to DPPC, indicating decreased area fraction of the disordered phase. All scale bars correspond to 5 μm.

giant unilamellar vesicles (GUVs) were electroformed using established protocols[2] and imaged under spinning disk confocal fluorescence microscopy. In the limit of high concentrations of the saturated lipid, where the lipid membrane was composed of over 80 mol% DPPC (Fig. 1a), we observed a single solid phase (Fig. 1b, composition 1, uniform distribution of probe lipid) as expected owing to the solubility of small amounts of cholesterol and low-melting temperature lipids in the solid phase.[52] Additionally, for vesicles containing a very high concentration of cholesterol and small amounts of the other two components (60 mol% cholesterol, 15 mol% DOTAP, 15 mol% DPPC), we observed a single liquid phase (Fig. 1b composition 2, uniform distribution of probe lipid), as expected based on the known ability of cholesterol to promote mixing of lipids with high and low melting temperatures.[52] For vesicles containing a very high concentration of DOTAP and small amounts of the other two components (80 mol% DOTAP, 10 mol% DPPC, 10 mol% cholesterol), we also observed a single liquid phase (Fig. 1b, composition 3, uniform distribution of probe lipid), suggesting that low concentrations of DPPC and cholesterol are soluble in DOTAP. For binary mixtures containing significant amounts of both DOTAP and DPPC (50–70 mol% DPPC, 30–50 mol% DOTAP) as well as for compositions containing only small amounts of cholesterol (45 mol% DPPC, 45 mol% DOTAP, 10 mol% cholesterol) we observed separation between liquid and solid phases, which is expected owing to the low miscibility of lipids with substantial differences in melting temperature.[52] Specifically, the probe lipid was concentrated within a portion of the surfaces of these vesicles, typically the majority, and excluded from another portion, typically the minority. Liquid–solid phase separation was characterized by the jagged edges of the border between the two phases as observed in Fig. 1b composition 4, indicating that the phase excluding the highly fluid probe molecule was sufficiently solid to overcome the influence of tension along the phase boundary, which favors smooth boundaries between liquid phases.[52]

Having established these limiting cases, we next examined the behavior of systems with nearly equivalent concentrations of the three components, DOTAP, DPPC, and cholesterol. Based on the established phase behavior of the DOPC/DPPC/cholesterol system, membranes with these compositions would be expected to separate into coexisting liquid-ordered and liquid-disordered phases, where the liquid-disordered phase is composed primarily of DOTAP and the liquid-ordered phase is composed primarily of cholesterol and DPPC.[52] The first composition we examined in this region contained 24 mol% DOTAP, 38 mol% cholesterol, and 38 mol% DPPC (Fig. 1b). A representative vesicle of this composition is shown in composition 5 of Fig. 1b. Here the vesicle separated into two distinct phases. In contrast to the jagged phase boundaries observed for compositions that separated into liquid and solid phases (Fig. 1b, composition 4), here phases were separated by a smooth boundary line, indicating that both phases were sufficiently fluid to be strongly influenced by tension along the boundary line, a commonly observed feature of systems that separate into co-existing liquid phases.[52]

Based on partitioning of the fluorescent probe, the majority phase appeared dark, indicating a less fluid composition, while the minority phase (30% of membrane surface area on average) appeared bright, indicating a more fluid composition. To determine whether DOTAP partitioned to the brighter, probe-rich phase or the dimmer, probe-poor phase, we examined the impact of increasing the molar fraction of DOTAP on the area fractions of the two phases. Specifically, vesicles composed of 50 mol% DOTAP, 20 mol% DPPC, and 30 mol% cholesterol, (composition 6 of Fig. 1b, Supplementary Fig. S1) also separated into two distinct phases separated by a smooth boundary, but, in contrast to composition 5, the fluid phase probe lipid favored the majority phase, which occupied on average 73% of the membrane surface. These results indicate that increasing the DOTAP content of membranes in the DOTAP/DPPC/cholesterol system increases the area fraction of the more liquid-like phase, indicating that DOTAP partitions into the liquid-disordered phase, as we expected based on its tail group chemistry.[52]

Having investigated the major regions of the DOTAP/DPPC/cholesterol phase diagram (Fig. 1b), we sought to optimize membrane composition in order to create vesicles that concentrated DOTAP within a small region of the membrane surface, which, as discussed above is expected to increase the efficiency of DOTAP as a driver of membrane fusion. Specifically, we examined the area fraction of the highly fluid DOTAP-containing phase as a function of the overall concentration of DOTAP. While maintaining a 1:1 ratio of DPPC to cholesterol we examined vesicles containing 24, 20, 16, 12, and 8 mol% DOTAP. The majority of vesicles for each of these compositions separated into a majority liquid-ordered phase (probe poor phase) and a minority liquid disordered phase (probe rich phase), as observed for composition 5 above. However, as the concentration of DOTAP was decreased, the area fraction of the disordered phase steadily decreased from $30 \pm 8\%$ (s.d.) for vesicles containing 24 mol% DOTAP to $7 \pm 3\%$ for vesicles containing 8 mol% DOTAP, all p values less than 0.003 (Figs. 1c, S2). These results establish that membrane phase separation can locally concentrate DO-

TAP within a highly fluid membrane phase of tunable area fraction (Fig. 1d). Having demonstrated this capability, we next sought to determine the impact of membrane phase separation on the efficiency of DOTAP-mediated membrane fusion.

Membrane Phase Separation Enhances DOTAP's Ability to Drive Lipid Mixing Between Model Membranes

The ability of two membrane surfaces to exchange lipids is a key first step in achieving membrane fusion.[44] Full membrane fusion ultimately results in mixing of molecules within the lumens of two initially separated membrane-bound volumes. This process of content-mixing will be examined later in the manuscript. However, as described in this section and the next, we began by characterizing the lipid mixing step. To examine the impact of membrane phase separation on lipid mixing, we formed DOTAP-containing small unilamellar vesicles (SUVs), which are lipid vesicles that range in diameter from 50 to 200 nm. We formed SUVs with both phase-separated and homogenous compositions, according to the phase diagram in Fig. 1b. All SUVs contained a trace amount of the fluorescent probe lipid, Texas Red-DPPE (0.3 mol%). To determine the extent to which each membrane composition promoted lipid mixing, SUVs of each composition were incubated with giant unilamellar vesicles (GUVs), which are lipid vesicles that are at least 1 μm in diameter, such that they can be easily resolved using fluorescence microscopy. GUVs consisted of the fluid lipid DOPC and a trace amount of the fluorescent probe, Oregon Green-DPPE (0.3 mol%) which is spectrally distinct from Texas Red. When SUVs and GUVs were mixed, significant transfer of lipids from the SUVs to a particular GUV was considered to have occurred if the Texas Red probe from the SUVs appeared uniformly distributed over the surface of the GUV in confocal fluorescence images, Fig. 2a. The extent to which a particular SUV composition was capable of promoting lipid mixing was then quantified by determining the fraction of GUVs that exhibited lipid transfer.

Phase-separated SUVs consisted of DPPC and cholesterol in a 1:1 molar ratio and 12, 16, or 24 mol% DOTAP. Notably, these SUVs are expected to be phase-separated and reflect the starting composition because these vesicles were heated above the melting temperature of DPPC to 65 °C during extrusion. Furthermore, at a diameter of approximately 200 nm, the curvature energy of these membranes is more than an order of magnitude below the enthalpy of mixing of the phase-separated membrane,[22,64] such that membrane curvature is unlikely to alter membrane phase behavior. For comparison, SUVs of four homogenous (i.e., not phase-separated) membrane compositions were examined: (i) 100 mol% DOPC which lacks DOTAP and was therefore the negative control, (ii) 20 mol% DOTAP and 80% DOPC, (iii) 24 mol% DOTAP and 76 mol% DOPC, and (iv) 100 mol% DOTAP, which is expected to be highly fusogenic[12] and was therefore the positive control. Notably, compositions (ii) and (iii) were homogenous as shown in Supplementary Fig. S3 because DOTAP and DOPC have the same tail group chemistry, making them highly miscible.

After formation and characterization, SUVs and GUVs were mixed together and incubated for 30 min at a ratio of approximately one to one in terms of total lipids per volume. Following incubation, each sample was imaged using spinning disk confocal fluorescence microscopy, where the fluorescence of the Texas Red and Oregon Green probes were visualized in distinct, non-overlapping fluorescence channels (see "Materials and Methods" section). As expected, the GUVs that were incubated with the negative control SUVs, 100 mol% DOPC, exhibited little evidence of lipid mixing. Specifically, Texas Red labeled SUVs were seen diffusing around GUVs, but had little interaction with GUV surfaces (Fig. 2b). GUVs exhibited only green fluorescence indicating no transfer of the Texas Red from the SUVs to the GUVs (Fig. 2b). Less than 1% of GUVs in these experiments exhibited lipid transfer from SUVs. In contrast, GUVs that were incubated with the positive control SUVs, 100 mol% DOTAP, exhibited strong evidence of lipid mixing. In these images, GUVs appear in both the Oregon Green and Texas Red channels with the probe lipids evenly distributed over the GUV surface (Fig. 2c). More than 80% of GUVs in these experiments exhibited lipid transfer from SUVs. Having established the behavior of the positive and negative controls, we next examined the behavior of GUVs exposed to either the phase-separated or homogenous SUVs as a function of DOTAP content.

Examining GUVs that were incubated with homogenous SUVs containing 24 mol% DOTAP, we observed behavior similar to the negative control. However, some SUVs were observed to stick to the GUV membrane, possibly owing to electrostatic interaction between the positive charge of DOTAP and the zwitterionic choline head group of DOPC in the GUVs.[5] However, in the majority of cases Texas Red did not appear to transfer from the SUVs to the membranes of the GUVs, suggesting that lipid mixing did not occur (Fig. 2d). Less than 10% of GUVs in these experiments exhibited lipid transfer from SUVs. In contrast, when phase-separated SUVs containing 24 mol% DOTAP were incubated with GUVs, the

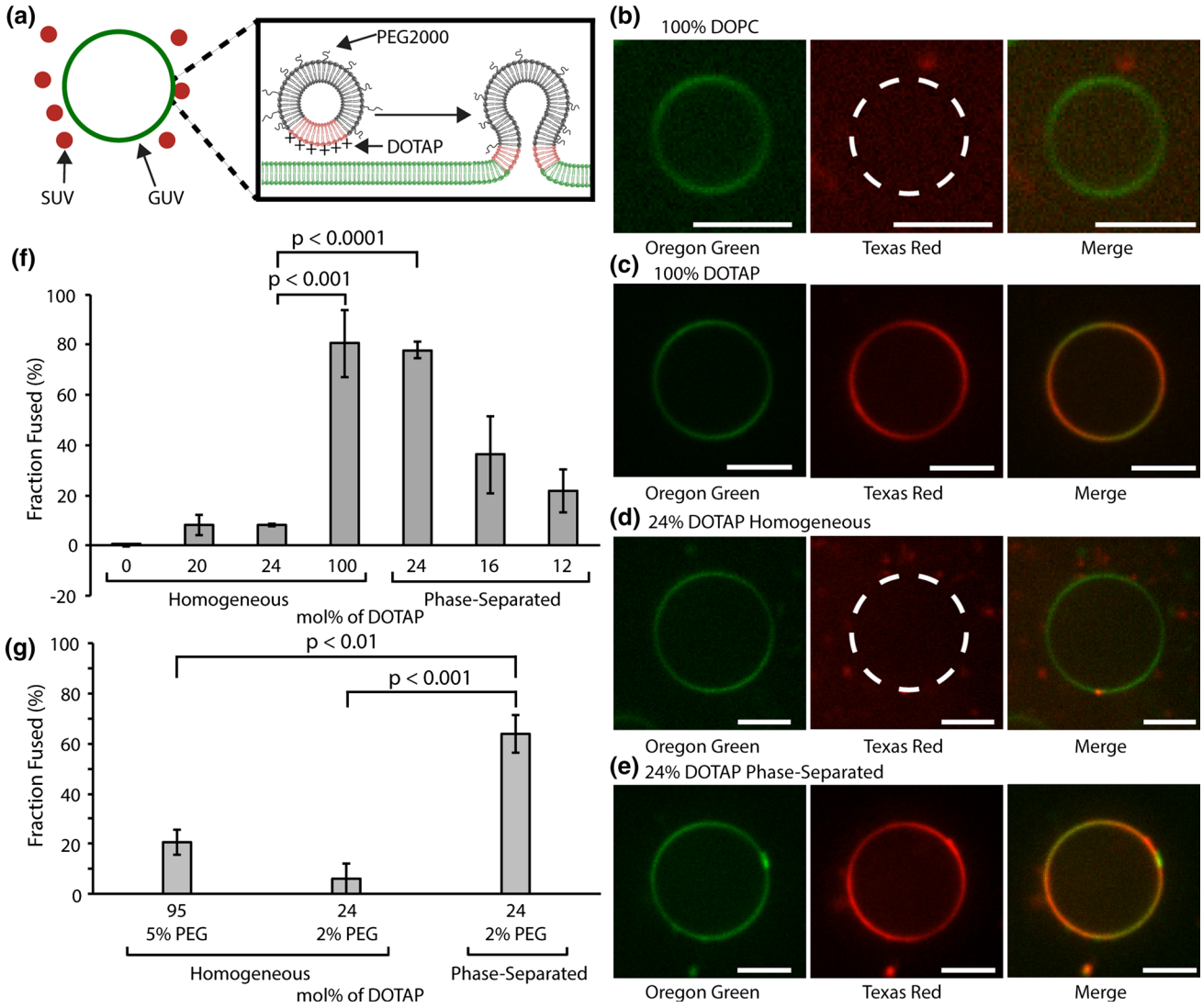

FIGURE 2. Membrane phase separation promotes lipid mixing in a model membrane assay. (a) Pictorial representation of phase-separated DOTAP containing SUVs fusing to a GUV. (b–e) Fluorescence confocal image slices of 100 mol% DOPC GUVs labeled with 0.3 mol% Oregon Green-DPPE incubated with (b) 100 mol% DOPC SUVs, (c) 100 mol% DOTAP SUVs, (d) Homogeneous 24 mol% SUVs (24 mol% DOTAP, 76 mol% DOPC), and (e) phase-separated 24 mol% SUVs (24 mol% DOTAP, 38 mol% cholesterol, 38 mol% DPPC) labeled with 0.3 mol% Texas Red-DPPE. All scale bars correspond to 5 μm. (f) Bar chart displaying the fraction of the GUV population that exhibited lipid transfer for each SUV composition (n = 3). Error bars correspond to the standard deviation. Brackets show statistically significant comparisons using an unpaired, 2-tailed student's t test. (g) Bar chart displaying the average fraction of GUVs exhibiting lipid transfer for each PEGylated SUV composition (n = 3). Error bars correspond to the standard deviation. Brackets show statistically significant comparisons using an unpaired, 2-tailed student's t test.

GUV membrane exhibited diffuse red fluorescence, indicating that the Texas Red-DPPE lipid had been transferred from the SUVs to the GUVs (Fig. 2e). Here the fraction of GUVs exhibiting lipid mixing increased as a function of the amount of DOTAP in the SUVs, from 22 ± 8% for SUVs containing 12 mol% DOTAP to 78 ± 3% for SUVs containing 24 mol% DOTAP (Fig. 2f). Comparing phase-separated and homogenous SUVs both containing 24 mol% DOTAP, GUVs exposed to phase-separated SUVs were approximately 8 times more likely to exhibit lipid mixing, p value less than 0.0001 (Fig. 2g). Collectively these results illustrate that the ability of DOTAP to drive lipid transfer was significantly increased when it was incorporated into a phase-separated membrane system.

We next sought to determine whether including a layer of polyethylene glycol (PEG) on SUV surfaces, as is frequently used on membrane surfaces to lengthen *in vivo* circulation,[26] would interfere with the membrane fusion process. When PEG was added to homogenous SUVs, lipid mixing was dramatically reduced. Specifically, when GUVs were exposed to SUVs consisting of 95 mol% DOTAP and 5 mol% PEGylated lipids

(PEG2000-DPPE), the fraction of GUVs exhibiting lipid mixing was only 20.9 ± 5.1% in comparison to 80.5 ± 13.5% for GUVs exposed to SUVs composed of 100 mol% DOTAP without PEG (Figs. 2f, 2g, S4). This result was expected since the hydrodynamic diameter of the PEG 2000 molecules that make up the passivating layer, a few nanometers, is comparable to or greater than the Debye length under physiological buffer conditions, such that DOTAP's charge should be significantly shielded by the PEG layer. In contrast, for phase-separated SUVs, the presence of the PEG layer did not substantially interfere with the fusion process. Specifically, when GUVs were exposed to phase-separated SUVs containing 24 mol% DOTAP, the fraction of GUVs exhibiting lipid mixing decreased only slightly from 77.9 ± 3.5% for SUVs without PEG to 63.8 ± 7.4% for SUVs containing 2 mol% PEGylated lipids (Figs. 2f, 2g, S4). Comparing GUVs exposed to both phase-separated and homogeneous 24 mol% DOTAP SUVs, the fraction of GUVs exhibiting lipid mixing was nearly 10 times higher when GUVs were exposed to phase-separated SUVs, p value less than 0.001. The results can be explained by the fact that the PEGylated lipid has saturated palmitoyl tails identical to those of the DPPC lipid, and has therefore been shown to partition preferentially to the liquid ordered majority phase,[25] while DOTAP partitions to the liquid-disordered minority phase, as described above. Therefore, the PEG layer is physically separated from DOTAP, likely preventing PEG from interfering with the lipid mixing process. Collectively, the data presented in Fig. 2 demonstrate that membrane phase separation enhances lipid mixing, a precursor to membrane fusion, between model membrane vesicles. We next sought to evaluate the extent to which phase separation impacts lipid mixing between SUVs and the membranes of live cells.

Membrane Phase Separation Enhances DOTAP-Mediated Lipid Mixing with Cells

We examined the impact of membrane phase separation on lipid transfer from DOTAP-containing SUVs to the membranes of live cells. In these studies, all phase-separated SUVs contained a 1:1 molar ratio of cholesterol to saturated lipids and either 24 or 15 mol% low melting temperature lipids, ensuring the formation of a well-defined liquid-disordered phase at the membrane surface, as described in Fig. 1 (Supplementary Fig. S5). However, to study the impact of DOTAP concentration on lipid transfer, we replaced some of the lipids in this phase with DOPC. As described above, DOPC has the same lipid tail chemistry as DOTAP, such that the two lipids are highly miscible and share a strong preference for the liquid-disordered phase. However, DOPC does not drive lipid mixing owing to its cylindrical shape and zwitterionic head group. Specifically, we considered the following ratios of DOTAP to DPPC within the low melting temperature lipid fraction: (i) 24% DOTAP/0% DOPC, (ii) 10% DOTAP/5% DOPC, and (iii) 5% DOTAP/10% DOPC. Our studies also examined three compositions of homogenous SUVs, which consisted of the miscible lipids DOTAP and DOPC, such that phase separation did not occur. All vesicles also contained 2 mol% PEG2000-DPPE, which is soluble in the DOPC/DOTAP mixture at this low concentration. The total concentration of DOTAP with homogenous SUVs matched that of phase-separated SUVs: (i) 24 mol% DOTAP, (ii) 10 mol% DOTAP, (iii) 5 mol% DOTAP. All SUVs, both homogenous and phase-separated contained the fluorescent probe lipid Oregon Green-DPPE (0.3 for 24 and 10 mol% DOTAP SUVs and 1 for 5 mol% DOTAP SUVs) to enable detection of lipid transfer in live cell imaging and flow cytometry assays.

We began by comparing the ability of phase-separated and homogenous SUVs, both containing 5 mol% DOTAP, to transfer the probe lipid to HeLa cells. SUVs were incubated with cells for 2 h followed by washing to remove excess SUVs, detachment of cells from the culture vessel using trypsin, and quantification of relative florescence using a flow cytometer equipped with an excitation source and emission filter appropriate for detecting the Oregon Green probe lipid (see "Materials and Methods" section).

Flow cytometry experiments were performed for three dose levels, 25, 125, and 250 μM of total SUV lipids in the solution surrounding the cells during incubation. The fluorescence emission of each group of cells was compared to that of untreated cells (n = 3). Cells incubated with 25 μM of SUVs showed no discernable shift in fluorescence after incubation with either phase-separated or homogeneous SUVs (Figs. 3a, 3c, S6). However, cells incubated with 125 or 250 μM of phase-separated SUVs exhibited significantly greater fluorescence emission in comparison to untreated cells (Figs. 3a, S6). In contrast, cells incubated with an equal concentration of homogenous SUVs exhibited only slightly greater fluorescence than untreated cells, such that the average increase in fluorescence for cells exposed to phase-separated SUVs in comparison to those exposed to homogenous SUVs, was 4 and 5 times greater for those exposed to phase-separated SUVs at lipid concentrations of 125 and 250 μM, respectively, p value less than 0.01 (Fig. 3c).

To confirm transfer or the probe lipid, Oregon Green-DPPE, to cells, we acquired fluorescence images of live cells incubated for 2 h with either phase-separated or homogenous SUVs, both containing 5 mol%

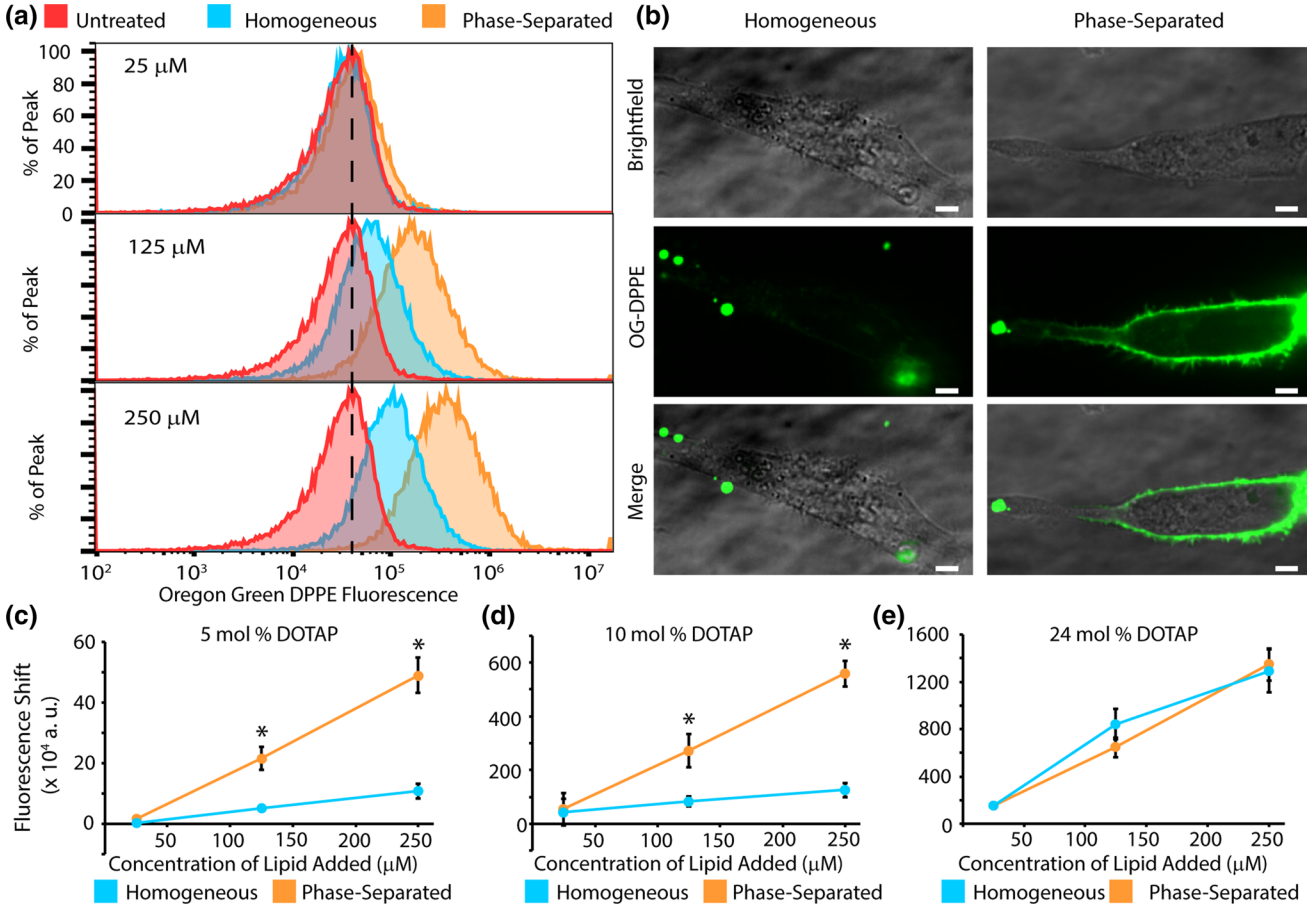

FIGURE 3. Membrane phase separation enhances lipid transfer from liposomes to cells. (a) Flow cytometry histograms showing Oregon Green-DPPE fluorescence for cells incubated with 25, 125, and 250 μM of each SUV condition. The vertical dashed line depicts the peak fluorescence of the untreated cell condition to illustrate the shift in relative Oregon Green-DPPE fluorescence. Each curve represents 3 independent, concatenated trials with a minimum 5000 cells analyzed per trial. (b) Fluorescence confocal image slices of HeLa cells incubated with both homogeneous and phase-separated vesicles. All scale bars correspond to 5 μm. (c, d) The change in average relative fluorescence as a function of increasing concentration of lipid added for cells incubated with (c) phase-separated (5 mol% DOTAP, 10 mol% DOPC, 42.5 mol% cholesterol, 39.5 mol% DPPC, 2 mol% PEG2000-DPPE, 1 mol% Oregon Green-DPPE) and homogenous (5 mol% DOTAP, 92 mol% DOPC, 2 mol% PEG2000-DPPE, 1 mol% Oregon Green-DPPE) 5 mol% DOTAP SUVs, (D) phase-separated (10 mol% DOTAP, 15 mol% DOPC, 42.5 mol% cholesterol, 40.5 mol% DPPC, 2 mol% PEG2000-DPPE, 0.3 mol% Oregon Green-DPPE) and homogenous (10 mol% DOTAP, 88 mol% DOPC, 2 mol% PEG2000-DPPE, 0.3 mol% Oregon Green-DPPE) 10 mol% DOTAP SUVs, (e) phase-separated (24 mol% DOTAP, 38 mol% cholesterol, 36 mol% DPPC, 2 mol% PEG2000-DPPE, 0.3 mol% Oregon Green-DPPE) and homogenous (24 mol% DOTAP, 74 mol% DOPC, 2 mol% PEG2000-DPPE, 0.3 mol% Oregon Green-DPPE) 24 mol% DOTAP SUVs. Each data point represents the average of 3 independent trials per condition. Error bars correspond to the standard deviation. An unpaired, 2-tailed student's *t* test was performed to determine statistical significance between homogeneous and phase-separated groups. Asterisks denote statistical significance $p < 0.01$.

DOTAP at a total lipid concentration of 125 μM. After incubation with phase-separated SUVs, Oregon green fluorescence was observed in the cellular plasma membrane, suggesting lipid transfer from the SUVs to the cell membrane (Fig. 3c). In contrast, after incubation with homogenous SUVs, cells did not exhibit fluorescence at the plasma membrane suggesting that dye transfer was much more limited. These imagining-based results are consistent with the findings from flow cytometry. Further a flow cytometry-based comparison of phase-separated and homogenous SUVs containing 10 mol% DOTAP yielded similar results, with phase-separated SUVs increasing cell fluorescence by 4–5 times in comparison to homogenous SUVs of equal DOTAP content, p value less than 0.01 (Figs. 3d, S7).

Surprisingly, when the total DOTAP concentration in SUVs was increased to 24%, the ability of SUVs to transfer the probe lipid to cells became approximately equivalent for phase-separated and homogenous SUVs (Figs. 3e, S8). This lack of sensitivity to membrane phase separation at high overall DOTAP content is in contrast to our findings in the model membrane system (Fig. 2) and may arise from enhanced lipid transfer to

cellular lipid membranes, which have a net negative charge that promotes interactions with DOTAP.[43] Specifically, when DOTAP concentration becomes high, vesicles may be strongly attracted to the cell membrane, leading to lipid transfer regardless of the enhancements in local surface concentration afforded by phase separation. However, these studies only examined lipid mixing and did not address content mixing, which depends on the more energetically demanding process of full fusion between SUV and cell membranes. Therefore, as explored in the next section, membrane phase separation may be important for full fusion and content delivery, even at DOTAP concentrations for which it is not required to achieve lipid mixing. Collectively data in this section indicate that lipid mixing between SUVs and live cells is enhanced by membrane phase separation at moderate DOTAP concentrations. We next sought to examine the impact of membrane phase separation on the transfer of large hydrophilic macromolecules to the cellular cytoplasm.

Membrane Phase Separation Enhances Macromolecular Delivery to Live Cells

Having demonstrated that membrane phase separation enhances the transfer of lipids from SUVs to cellular membranes, we next examined the extent to which membrane phase separation could enhance the transfer of hydrophilic macromolecules to the cellular cytoplasm. Specifically, we formed phase-separated GUVs containing a model hydrophilic macromolecule, a fluorescent-labeled dextran polymer of 10–20 kDa molecular weight, which lacks significant membrane permeability.[29,50] In these experiments, we chose to deliver dextran using DOTAP-containing GUVs, rather than SUVs, since the large volume that can be encapsulated within GUVs, approximately 1000 times more than in a population of SUVs made from the same total mass of lipids, greatly facilitated unambiguous fluorescence-based detection of macromolecules in the cellular cytoplasm. Notably, GUVs are on the micron scale and would therefore not be appropriate for *in vivo* studies.

Both homogeneous and phase-separated GUVs containing dextran were formed using an established protocol.[32] Homogeneous GUVs contained 24 mol% DOTAP, 2 mol% PEG2000-DPPE, and 74 mol% DOPC, while phase-separated GUVs contained 24 mol% DOTAP, 2 mol% PEG2000-DPPE, 36 mol% DPPC, and 38 mol% cholesterol. The GUVs were labeled with a trace amount of the membrane dye, Oregon Green-DPPE (1 mol%), and were electroformed in the presence of 20 kDa TRITC-dextran at a concentration of 1.5 mM. After the vesicles were formed, free dextran was removed by several cycles of pelleting the GUVs using light centrifugation followed by resuspension in fresh, isosmotic buffer.

In confocal fluorescence images, it was clear that GUVs encapsulated TRITC-dextran and were phase-separated (Fig. 4a). Specifically, phase-separated GUVs exhibited two distinct phases in the Oregon Green fluorescence channel (Fig. 4a), a majority phase that appeared bright and a minority phase that appeared dark. Notably, Oregon Green DPPE is known to partition preferentially to liquid-ordered phases,[37] the opposite of the Texas Red DPPE probe lipid used in Fig. 1, which partitions preferentially to liquid disordered phases. Therefore, it is expected that the minority, DOTAP-rich phase appears dark in images contrasted with Oregon Green DPPE. The fluorescence of TRITC-dextran was seen in the lumen of both phase-separated and homogeneous GUVs indicating that TRITC-dextran was successfully loaded (Fig. 4a). Additionally, the lack of significant red fluorescence in the area outside of the GUVs indicated that free dextran was successfully removed (Fig. 4a). Furthermore, when observing the red and green fluorescence channels simultaneously, little TRITC-dextran signal was seen in the lipid membrane suggesting that the dextran did not interact strongly with the lipid membrane (Fig. 4a).

Having demonstrated the ability to load both phase-separated and homogenous GUVs with dextran, we next examined the ability of the GUVs to deliver the encapsulated dextran to cells. Dextran loaded GUVs with Oregon Green-DPPE labeled membranes were synthesized and washed *via* centrifugation. Next, the GUVs were incubated with HeLa cells for 2 h before spinning disk confocal images were acquired. Cells that were incubated with phase-separated GUVs exhibited a strong Oregon Green fluorescence signal in the plasma membrane, indicating that lipids were transferred from GUVs to the cell membrane (Fig. 4b). Furthermore, dextran fluorescence was observed in the interior of the cells (Fig. 4b). In contrast, cells incubated with dextran loaded GUVs that lacked DOTAP (pure DOPC), cellular membranes did not exhibit strong Oregon Green fluorescence and the cellular interior had lower levels of dextran fluorescence (Fig. 4b). While these images show that phase separated GUVs accomplished lipid delivery to cells it was challenging to determine whether dextran was delivered to the cell cytoplasm or simply trapped within the cell's endomembrane system.

To address this question, we devised a novel assay of cytoplasm content that relies on the extraction of membrane blebs from cells. Plasma membrane blebs are micron-scale spherical vesicles that form during contraction of the actin cortex in cellular processes such as cytokinesis, apoptosis, and cell crawl-

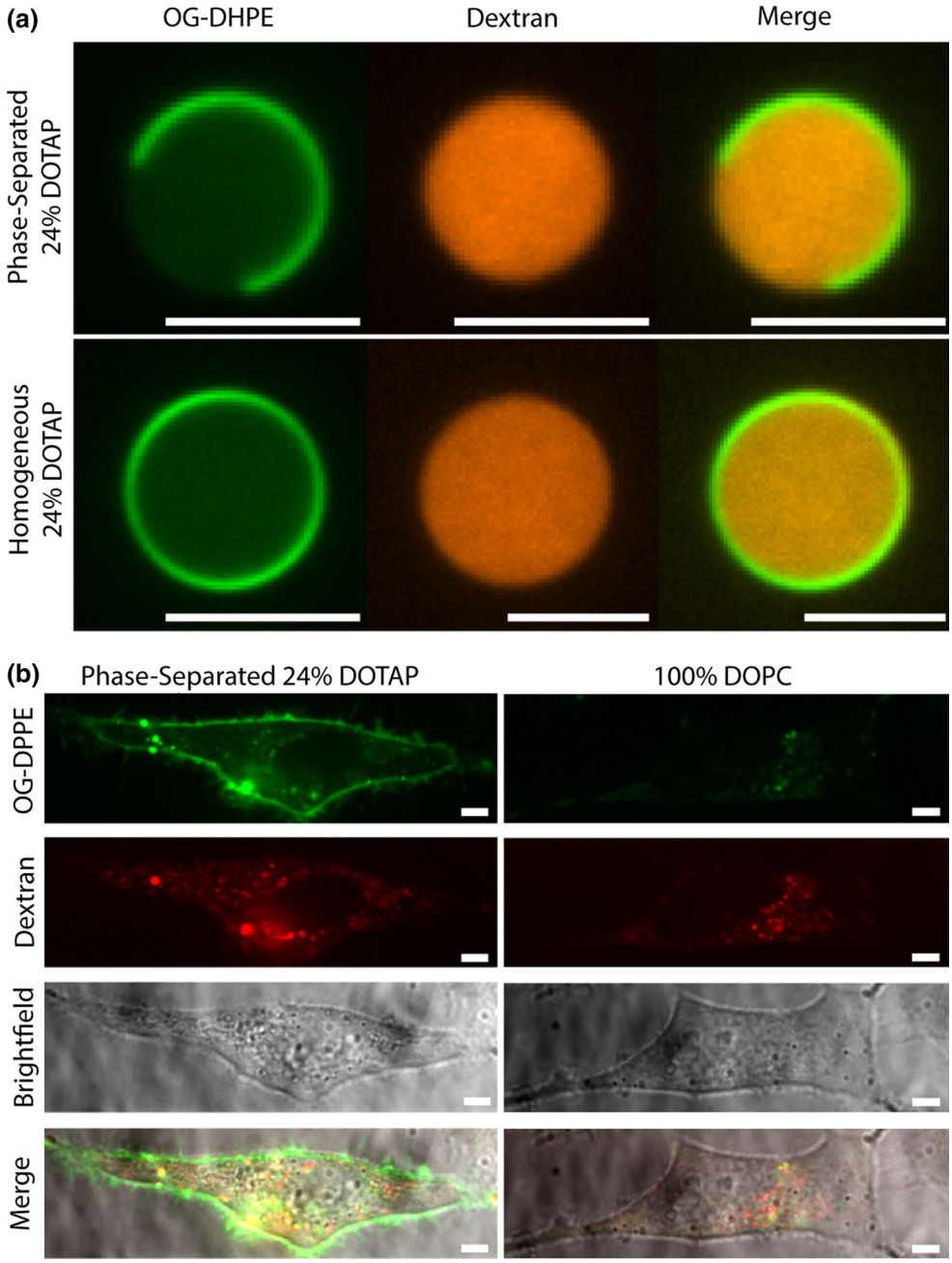

FIGURE 4. Formation of dextran-loaded GUVs and their exposure to cells. (a) Fluorescence confocal image slices of phase-separated (24 mol% DOTAP, 38 mol% cholesterol, 36 mol% DPPC, 2 mol% PEG2000-DPPE) and homogeneous (24 mol% DOTAP, 74 mol% DOPC, 2 mol% PEG2000-DPPE) GUVs loaded with 20,000 Da TRITC-dextran (red) and labeled with 1 mol% Oregon Green-DPPE (green). (b) Fluorescence confocal image slices of HeLa cells that were incubated with phase-separated 24 mol% DOTAP GUVs (24 mol% DOTAP, 38 mol% cholesterol, 36 mol% DPPC, 2 mol% PEG2000-DPPE) and homogeneous 100 mol% DOPC GUVs loaded with 10,000 Da Rhodamine B-dextran (red) and labeled with Oregon Green-DPPE (1 mol%) (green). All scale bars correspond to 5 μm.

ing.[6,7,15,35,40] The membrane of a bleb is composed of the cellular plasma membrane and the bleb lumen is derived from the cellular cytoplasm. Importantly, blebs do not contain organelles, such that all molecules encapsulated within a bleb are derived from the cell cytoplasm. Therefore, if fluorescent dextran is successfully delivered to the cytoplasm of a cell, then we would expect to detect dextran fluorescence within the lumen of blebs extracted from that cell.

So that the morphology of the cellular plasma membrane could be visualized, these experiments were performed using a HeLa cell line that stably expressed a

membrane-bound green fluorescing protein (GFP) domain. As described in the methods section, GFP was expressed as an N-terminal fusion to the transmembrane domain of the transferrin receptor, such that the cellular plasma membrane, and to a lesser extent, the cell's internal membranes were highlighted (Fig. 5a). These cells were incubated with TRITC-dextran loaded, phase-separated GUVs for 2 h (Fig. 5a). After incubation, the cells were washed to remove any remaining GUVs. Then plasma membrane blebs were extracted from these cells by exposing them to a hypoosmotic buffer containing a low concentration of fixative[47] (see "Materials and Methods" section). After 2 h of exposure to this buffer, the cells were imaged to visualize membrane blebs attached to the cell surface (Fig. 5a). The images revealed spherical plasma membrane blebs labeled by membrane-bound GFP and attached to the surfaces of cells, which contained a strong dextran fluorescence signal in their luminal space (Fig. 5b). In addition to the strong dextran fluorescence signal in the cytoplasm and blebs, there are visible puncta of dextran within the cells, which may indicate that vesicles deliver dextran through fusion with endosomal membranes as well as direct fusion with the cellular plasma membrane. Notably, endosomal fusion is likely enhanced by the increased fusogenic potential of DOTAP in the low pH environment of the endosome.[38,57] Fusion of vesicles with either the plasma membrane or the endosomal membrane both lead to release of vesicle contents into the cytoplasm,[38,49] making both pathways useful for delivery (Supplementary Figs. S9, S10). Very similar blebs were formed from cells exposed to homogenous GUVs containing 50 mol% DOTAP and 50 mol% DOPC (Fig. 5b). These experiments establish that DOTAP-containing GUVs are capable of transferring encapsulated dextran polymers to the cytoplasm of cells. Notably, during the delivery process, some of the dextran encapsulated by the vesicles is likely released into the surrounding media through either vesicle rupture or leakage during fusion with cellular membranes. However, as a hydrophilic macromolecule, dextran lacks membrane permeability and therefore cannot enter the cell cytoplasm without the aid of membrane permeating agents.[29,50] We next employed flow cytometry to determine the extent to which the delivery of dextran depended upon membrane phase separation.

In flow cytometry experiments, HeLa cells were incubated with approximately 100 μM (total lipid) of dextran loaded GUVs for 2 h, followed by washing, trypsonization, and preparation for flow cytometry. The precise concentration of GUVs was adjusted in order to maintain an equivalent total dose of fluorescent dextran molecules across all experiments, as determined by measurement of the fluorescence inten-

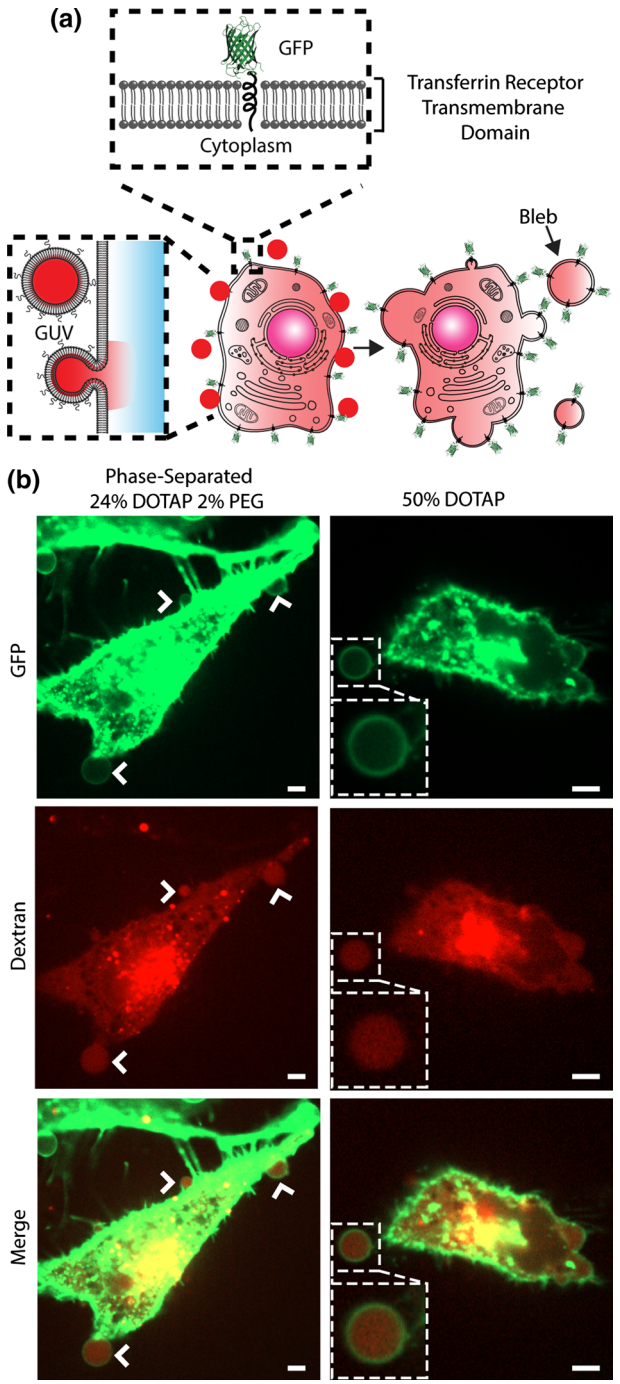

FIGURE 5. Extraction of cellular blebs confirms the delivery of hydrophilic macromolecules to the cellular cytoplasm. (a) Cartoon illustrating the structure of membrane bound GFP (top), the processes of macromolecular delivery by GUVs (left), and extraction of cellular blebs (right). (b) Fluorescence confocal image slices of GFP expressing HeLa cells (green) that were incubated for 2 h with fusogenic phase-separated GUVs (24 mol% DOTAP, 38 mol% cholesterol, 36 mol% DPPC 2 mol% PEG2000-DPPE) and fusogenic homogeneous GUVs (50 mol% DOTAP, 50 mol% DOPC) loaded with 20,000 Dalton TRITC-dextran (red) and were then induced to release cellular blebs. Arrows indicate dextran-filled blebs at the cellular membrane surface, illustrating that dextran is present in the cellular cytoplasm. All scale bars correspond to 5 μm.

sity of GUV samples after washing to remove unencapsulated fluorescent dextran. Four conditions were tested: (i) untreated cells, (ii) cells exposed to homogeneous 100 mol% DOPC GUVs which served as the negative control, (iii) cells exposed to homogeneous 24 mol% DOTAP 2% PEG2000-DPPE GUVs, and (iv) cells exposed to phase-separated 24 mol% DOTAP 2% PEG2000-DPPE GUVs. Cells treated with dextran-loaded DOPC GUVs experienced a small shift in fluorescence, indicating little delivery of dextran to the cytoplasm, consistent with imaging results in Fig. 6a. In contrast, the flow cytometry histograms indicated a large shift in red fluorescence for cells incubated with TRITC-dextran loaded phase-separated GUVs (Figs. 6a, S11), approximately 40 times higher than the average relative red fluorescence of untreated cells, p value less than 0.02 (Fig. 6b). By comparison, the shift in relative red fluorescence observed in the cells incubated with homogeneous GUVs (Fig. 6a), was only 10 times greater than untreated cells, p value less than 0.02 (Fig. 6b). Notably, further increasing the concentration of DOTAP in homogeneous vesicles did not dramatically impact fusion (Supplementary Fig. S12). Collectively, these results demonstrate that membrane phase separation substantially increases the ability of the fusogenic lipid, DOTAP, to deliver hydrophilic macromolecules to cells.

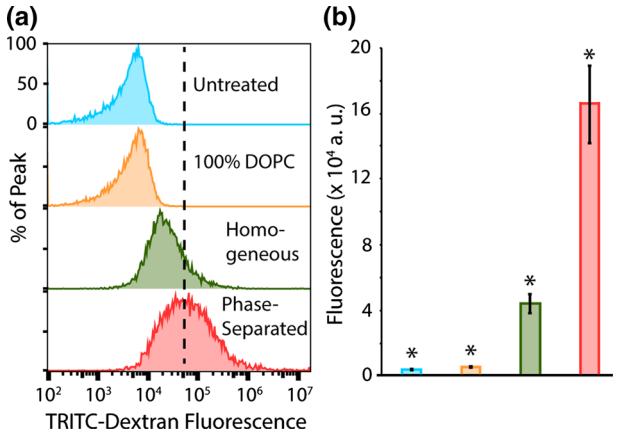

FIGURE 6. Phase separation enhances macromolecular delivery to live cells. (a) Flow cytometry histograms showing relative fluorescence of cells incubated with approximately 100 μM (total lipid) of GUVs loaded with 20,000 Da TRITC-dextran. The dashed line is centered on the peak fluorescence (60,000 fluorescence a.u.) of cells exposed to 24 mol% DOTAP 2 mol% PEG2000-DPPE phase-separated GUVs (24 mol% DOTAP, 38 mol% cholesterol, 36 mol% DPPC, 2 mol% PEG2000-DPPE). Each curve represents 3 independent, concatenated trials with a minimum of 5000 cells analyzed per trial. (b) Average red fluorescence in treated and untreated cells (n = 3). Error bars correspond to the standard deviation of all trials. Asterisks demonstrate that all differences between each data were statistically significant ($p < 0.02$) using an unpaired, 2-tailed student's t test. The color of the bar corresponds to the legend shown in (a).

CONCLUSIONS

Here we have demonstrated that membrane phase separation can substantially enhance fusion of DOTAP containing vesicles to target membranes. Specifically, our experiments demonstrate that membrane phase separation enhances the ability of DOTAP-containing liposomes to transfer lipids to model membranes by a factor of 8–10 in comparison to homogenous vesicles, and to cells by a factor of 4–5 in comparison to homogenous vesicles. Additionally, we have demonstrated that phase separated vesicles transfer the model macromolecule, dextran, to the cellular cytoplasm 4 times more efficiently than homogenous vesicles. These phase-separated membrane systems show promise in overcoming the obstacle of macromolecular delivery to the cellular cytoplasm. Specifically, we show that membrane phase separation reduces the total amount of DOTAP required for fusion to as little as 5 mol%. In contrast, existing DOTAP-containing delivery systems typically employ 50–100% DOTAP to achieve fusion.[56,65]

An immediate application of these results is that the concentration of DOTAP, or similar fusion-promoting lipids, required to drive macromolecular delivery can be substantially reduced by incorporating DOTAP in a phase separating lipid mixture, leading to greater cell viability and reduced toxicity. In the future, membrane phase separation and subsequent membrane fusion could be triggered by exposure of liposomes to target cell populations. We envision two possible mechanisms for triggering phase separation. First, phase separation could be triggered by ligand binding.[18,60] In particular, phase-separated liposomes could incorporate ligands that bind specifically to receptors expressed at high levels by a target cell population. Binding of vesicles to these cells would locally concentrate specific lipids, reducing the energetic cost of membrane phase separation, as has been demonstrated in fundamental membrane studies.[18,60] By optimizing the membrane phase transition for sensitivity to this subtle shift in liposome composition, membrane phase separation and subsequent membrane fusion could be accomplished in a target-cell dependent manner. Second, phase separation could be triggered by pH-dependent shedding of a crowded PEG layer. Previous work done in our group has shown that crowded polymer molecules on the surface of a lipid membrane generate steric pressure that prevents membrane phase separation from taking place.[25] However, once the crowded PEG layer is removed, phase separation can occur. Therefore, by incorporating a cleavable PEG layer on the surfaces of our liposomes, we could

create liposomes that are initially passivated by PEG but become phase-separated and fusogenic when the PEG layer is removed. Several groups have recently developed PEG-conjugated lipids and surfactants that can be cleaved by the reduced pH of endosomal compartments or the tumor micro-environment.[61–63] By incorporating these reagents into our liposomes, we could construct an efficient, pH-activated membrane fusion system. Collectively, this work harnesses membrane phase separation to substantially improve the efficiency of DOTAP-mediated membrane fusion, a key first step toward building an efficient and controllable system for the delivery of hydrophilic macromolecules to the cellular cytoplasm.

MATERIALS AND METHODS

Chemical Reagents

DTT (dithiothreitol), PFA (paraformaldehyde), NaCl, $CaCl_2$, HEPES (4-(2-hydroxyethyl)-1-piperazineethanesulfonic acid, polybrene, puromycin, Rhodamine B isothiocyanate-dextran with an average molecular weight of 10,000 Da (Rhodamine B-dextran) and Tetramethylrhodamine isothiocyanate-dextran with an average molecular weight of 20,000 Da (TRITC-dextran) were purchased from Sigma Aldrich. Sucrose and hydrochloric acid (HCl) were purchased from Fisher Scientific. Fetal bovine serum (FBS), trypsin, penicillin, streptomycin, L-glutamine, PBS (phosphate buffered saline), and DMEM (Dulbecco's modified Eagle medium) were purchased from GE Healthcare. Texas Red-DPPE (Texas Red-1,2-dipalmitoyl-*sn*-glycero-3-phosphoethanolamine) and Oregon Green-DPPE (Oregon Green-1,2-Dipalmitoyl-*sn*-glycero-3-phosphoethanolamine) were purchased from Thermofisher. Fugene was purchased from Promega. Trypan blue was purchased from Life Technologies. DPPC (1,2-dipalmitoyl-*sn*-glycero-3-phosphocholine), DOPC (1,2 dioleoyl-*sn*-glycero-3-phosphocholine), cholesterol (from ovine wool), DOTAP (1,2 dioleoyl–3-trimethylammonium-propane), PEG2000-DPPE (1,2 dipalmitoyl-*sn*-glycerol-3-phosphoethanolamine-N-[Methoxy(Polyethylene glycol)-2000]) were all purchased from Avanti Polar Lipids (Alabaster, AL). All reagents were used without further purification.

Giant Unilamellar Vesicles

Giant Unilamellar Vesicle (GUV) electroformation was completed by following published protocol.[2] Target GUVs were composed of 100% DOPC. The lipids were spread on inidium-tin-oxide (ITO) coated glass slides (resistance ~ 8–12 Ω-sq^{-1}) and were placed in a vacuum desiccator for at least 2 h to remove all of the solvent. The vesicles were prepared using a 310-milliosmole sucrose solution. The electroformation oven was set to approximately 55 °C to exceed the melting temperature of DPPC, 41 °C. After electroformation, the vesicle solution osmolarity was measured using a vapor pressure osmometer (Wescor). TRITC-dextran loaded vesicles were electroformed following an established protocol.[32] After vacuum desiccation, the dried lipids were prepared using a 4 mM HEPES, 250 mM Sucrose buffer containing 30 mg mL^{-1} of TRITC-dextran.

Washing Dextran-Loaded Giant Unilamellar Vesicles (GUV)

After electroformation, unencapsulated dextran was removed from the GUVs *via* a centrifugation washing protocol. Briefly, 200 μL of vesicle solution was diluted in 800 μL of 20 mM HEPES 150 nM NaCl pH 7.4 buffer then centrifuged at 100×*g* for 3 min to pellet the GUVs. 800 μL of supernatant containing free dextran was removed and 800 μL of fresh buffer was added gently as to not disturb the pelleted GUVs. This process was repeated 4 times. After the final centrifugation 200 μL of 20 mM HEPES 150 mM NaCl pH 7.4 buffer was added to solution and the GUV pellet was resuspended to a final volume of 400 μL. The fluorescence emission of the sample was then measured using a Cytation 3 Multi-Mode Reader (BioTek) to ensure that an equivalent dose of dye was incubated with target membranes.

Small Unilamellar Vesicles

Small Unilamellar Vesicles (SUVs) were extruded using a mini-extruder (Avanti). First, lipids were mixed and dried using N_2 gas and placed under vacuum for a minimum of 2 h. Vesicles were swelled for 30 min at 37 °C then extruded through 200-nm (171 ± 16 nm by dynamic light scattering) polycarbonate filters (VWR) for a minimum 21 passes at 65 °C. A Zetasizer Nano ZS (Malvern) was used for dynamic light scattering measurements.

Microscopy

Spinning disk confocal microscopy (Zeiss Axio Observer Z1 with Yokagawa CSU-X1M) was used to image GUVs and cells. Laser wavelengths of 488 and 561-nm were used for excitation. The bandpass emission filters were centered at 525 with 50-nm bandwidth, and 629 with 62-nm bandwidth. Plan-Apochromat 100× 1.4 numerical aperture and a Plan-Apochromat 63× 1.4 numerical aperture oil objectives were used. A

cooled (−70 °C) EMCCD iXon3 897 camera was used for imaging (Andor Technology). For cell experiments, cells were cultured on acid cleaned 22-mm square coverslips (Fisherbrand).

Acid Cleaning Coverslips

22 × 22 mm glass coverslips (Fisherbrand) were heated at 60 °C in 1 M HCl in a covered glass beaker for approximately 10 h, and allowed to cool to room temperature. Distilled water was used to rinse coverslips. Next, coverslips were placed in distilled water in a covered glass beaker and sonicated in a bath sonicator for 15 min 3 times. After sonication in distilled water, the coverslips were sonicated in 50% ethanol and 50% distilled water for 15 min, then in 70% ethanol and 30% distilled water for 15 min, and finally 95% ethanol and 5% distilled water for 15 min. Coverslips were then stored in 95% ethanol and 5% distilled water.

Imaging Slide Preparation

Vesicles were diluted by a factor of 6 in 20 mM HEPES, 150 mM NaCl pH 7.4 buffer raised to a final osmolarity of approximately 300 mOsm by the addition of sucrose. The slight osmotic tension suppressed membrane fluctuations, improving image quality and results reproducibility. In all cases vesicles were observed in small, sealed, disposable chambers composed of 24 × 40 mm glass cover slips (fisherbrand) and spacers made from 3 layers of double sided tape. For SUV to GUV fusion experiments, SUVs were introduced to GUVs at a 1.25:1 SUV to GUV ratio based on total lipid concentration and incubated together at room temperature for 30 min before imaging. Approximately 5 min before imaging, the samples were prepared to allow GUVs to settle to the bottom of the coverslip.

Estimating the Area Fraction of DOTAP-rich Lipid Domains

The average area of the DOTAP-enriched domain as a percentage of total vesicle surface area was estimated using 3D confocal reconstructions of the vesicle. From these reconstructions the domain was considered to be a spherical cap for which the area was calculated based on measurements of the vesicle diameter and the cap diameter.

Determining the Fraction of GUVs Exhibiting Lipid Mixing

Data were collected from three independent batches of GUVs. Ten image stacks per experimental condition were taken, each containing multiple GUVs. A minimum of 70 GUVs per batch were counted per data point. The fraction of GUVs exhibiting lipid mixing was determined by calculating the number of GUVs exhibiting diffuse red and green fluorescence at the membrane perimeter as a percentage of the total population of GUVs in an image. To be counted as a GUV, the vesicle had to be at least 4 μm in diameter and lack a significant amount of luminal debris.

Cell Culture and Stable Cell Line Development

HeLa cells were purchased from American Type Culture Collection (ATCC). The GFP tagged surface receptor HeLa cells were produced *via* lentiviral transfection. The GFP-tagged receptor gene sequence was sub-cloned onto pLJM1 viral transfer vector (addgene #19319) with NheI and EcoRI sites. Lentiviruses were generated by co-transfecting the transfer plasmid, packaging plasmid Δ8.9 and the envelope plasmid VSVG into 293T packaging cells with FuGENE. 48 h after the transfection, virus-containing supernatant was collected, filtered and added to HeLa cells with 8 μg mL^{-1} of polybrene. Transduced HeLa cells were selected with 2 μg mL^{-1} puromycin for 7 days. All cells were cultured in DMEM high glucose supplemented with 10% FBS and 1% penicillin, streptomycin, and L-glutamine (PSLG). All cells were incubated at 37 °C with 5% CO_2 and passaged every 48–72 h. For fluorescence microscopy cells were grown on acid-cleaned 22 × 22 mm glass coverslips (Fisherbrand) in 6-well plates(Corning) for 24 h. For flow cytometry cells were grown in 96-well plates (Corning) for 24 h.

Flow Cytometry

An Accuri C6 Flow Cytometer (BD Biosciences) with 488 and 551 nm excitation lasers was used for all flow cytometry experiments. For lipid mixing experiments with Oregon Green-DPPE, phase-separated and homogeneous SUVs with a molar concentration of DOTAP greater than 10 mol% saturated the 575 ± 25 nm bandpass filter. Therefore, a 610 ± 20 nm bandpass filter was used to analyze this data. Oregon Green-DPPE labeled vesicles composed of 5 mol% DOTAP were analyzed using the 575 ± 25-nm bandpass filter. To compare the flow cytometry data collected from vesicles composed of 10 and 24 mol% DOTAP to data collected for vesicles composed of 5 mol% DOTAP, the fluorescence ratio between the 610 nm filter and the 575 nm filter was determined. This ratio, approximately 29 fold, was calculated by dividing the median fluorescence detected by the 575 nm bandpass filter by the median fluorescence detected by the 610 nm bandpass filter for a given condition. For content mixing experiments with TRITC-dextran, a

586 ± 15 nm bandpass filter was used. All data were collected at 35 μL min^{-1}. The gate was drawn to contain the majority population of the forward scattering vs. side scattering plot on untreated cells and applied to all experiments with the same cell type. All flow cytometry data were analyzed using FlowJo (Treestar).

Giant Plasma Membrane Vesicles

After incubation with dye loaded GUVs, Giant Plasma Membrane Vesicles (GPMVs) were derived from donor cells. According to published protocols, donor cells were washed twice with GPMV buffer (10 mM HEPES, 2 mM $CaCl_2$, 150 mM NaCl, pH 7.4) and once with GPMV active buffer (10 mM HEPES, 2 mM $CaCl_2$, 150 mM NaCl, 25 mM PFA, 1 mM DTT, pH 7.4). Then the cells were incubated in active buffer at 37 °C with 5% CO_2 for 2 h before imaging.

ELECTRONIC SUPPLEMENTARY MATERIAL

The online version of this article (doi:10.1007/s12195-017-0489-4) contains supplementary material, which is available to authorized users.

ACKNOWLEDGMENTS

This work was supported by the National Science Foundation Division of Materials Research (DMR 1352487 to Stachowiak) and also National Institute of General Medical Science (Grant No. GM112065). We thank the BME Community of Undergraduate Research Scholars for Cancer (BME CUReS Cancer) an NSF sponsored Research Experience for Undergraduates (REU) at The University of Texas at Austin for enabling Grant Ashby to work in the Stachowiak Laboratory at UT Austin. We thank the laboratories of Professors Aaron Baker and Janet Zoldan for assistance with lentiviral transfection.

CONFLICT OF INTEREST

All authors, including Z. I. Imam, L. E Kenyon, G. Ashby, F. Nagib, M. Mendicino, C. Zhao, A. K. Gadok, and J. C. Stachowiak, declare that they have no conflict of interest.

ETHICAL APPROVAL

No human studies were carried out by the authors for this article. No animal studies were carried out by the authors for this article.

REFERENCES

[1]Alvarez-Erviti, L., Y. Q. Seow, H. F. Yin, C. Betts, S. Lakhal, and M. J. A. Wood. Delivery of siRNA to the mouse brain by systemic injection of targeted exosomes. *Nat. Biotechnol.* 29:341–345, 2011.

[2]Angelova, M. I., and D. S. Dimitrov. Liposome Electroformation. *Faraday Discuss.* 81:303–311, 1986.

[3]Baker, A. H., A. Kritz, L. M. Work, S. A. Nicklin, and A. Nicklin. Cell-selective viral gene delivery vectors for the vasculature. *Exp. Physiol.* 90:27–31, 2005.

[4]Batrakova, E. V., and M. S. Kim. Using exosomes, naturally-equipped nanocarriers, for drug delivery. *J. Controll. Release* 219:396–405, 2015.

[5]Blosser, M. C., J. B. Starr, C. W. Turtle, J. Ashcraft, and S. L. Keller. Minimal effect of lipid charge on membrane miscibility phase behavior in three ternary systems. *Biophys. J.* 104:2629–2638, 2013.

[6]Charras, G. T., M. Coughlin, T. J. Mitchison, and L. Mahadevan. Life and times of a cellular bleb. *Biophys. J.* 94:1836–1853, 2008.

[7]Charras, G. T., C. K. Hu, M. Coughlin, and T. J. Mitchison. Reassembly of contractile actin cortex in cell blebs. *J. Cell Biol.* 175:477–490, 2006.

[8]Chazal, N., and D. Gerlier. Virus entry, assembly, budding, and membrane rafts. *Microbiol. Mol. Biol. Rev.* 67:226–237, 2003.

[9]Choi, K. S., H. Aizaki, and M. M. C. Lai. Murine coronavirus requires lipid rafts for virus entry and cell-cell fusion but not for virus release. *J. Virol.* 79:9862–9871, 2005.

[10]Chollet, P., M. C. Favrot, A. Hurbin, and J. L. Coll. Side-effects of a systemic injection of linear polyethylenimine-DNA complexes. *J. Gene Med.* 4:84–91, 2002.

[11]Ciani, L., A. Casini, C. Gabbiani, S. Ristori, L. Messori, and G. Martini. DOTAP/DOPE and DC-Chol/DOPE lipoplexes for gene delivery studied by circular dichroism and other biophysical techniques. *Biophys. Chem.* 127:213–220, 2007.

[12]Ciani, L., S. Ristori, L. Calamai, and G. Martini. DOTAP/DOPE and DC-Chol/DOPE lipoplexes for gene delivery: zeta potential measurements and electron spin resonance spectra. *Biochim. Biophys. Acta Biomembr.* 1664:70–79, 2004.

[13]Egleton, R. D., and T. P. Davis. Bioavailability and transport of peptides and peptide drugs into the brain. *Peptides* 18:1431–1439, 1997.

[14]Filion, M. C., and N. C. Phillips. Toxicity and immunomodulatory activity of liposomal vectors formulated with cationic lipids toward immune effector cells. *Biochim. Biophys. Acta Biomembr.* 1329:345–356, 1997.

[15]Friedl, P., and K. Wolf. Tumour-cell invasion and migration: diversity and escape mechanisms. *Nat. Rev. Cancer* 3:362–374, 2003.

[16]Futami, J., M. Kitazoe, T. Maeda, E. Nukui, M. Sakaguchi, J. Kosaka, M. Miyazaki, M. Kosaka, H. Tada, M. Seno, Y. Sasaki, N. H. Huh, M. Namba, and H. Yamada. Intracellular delivery of proteins into mammalian living cells by polyethylenimine-cationization. *J. Biosci. Bioeng.* 99:95–103, 2005.

[17]Gibbs, J. B. Mechanism-based target identification and drug discovery in cancer research. *Science* 287:1969–1973, 2000.

[18]Gordon, V. D., M. Deserno, C. M. J. Andrew, S. U. Egelhaaf, and W. C. K. Poon. Adhesion promotes phase separation in mixed-lipid membranes. *EPL* 84:48003, 2008.

[19]Grakoui, A., S. K. Bromley, C. Sumen, M. M. Davis, A. S. Shaw, P. M. Allen, and M. L. Dustin. The immunological synapse: a molecular machine controlling T cell activation. *Science* 285:221–227, 1999.
[20]Gunawan, R. C., and D. T. Auguste. Immunoliposomes that target endothelium in vitro are dependent on lipid raft formation. *Mol. Pharm.* 7:1569–1575, 2010.
[21]Gunawan, R. C., and D. T. Auguste. The role of antibody synergy and membrane fluidity in the vascular targeting of immunoliposomes. *Biomaterials* 31:900–907, 2010.
[22]Hac, A. E., H. M. Seeger, M. Fidorra, and T. Heimburg. Diffusion in two-component lipid membranes—a fluorescence correlation spectroscopy and Monte Carlo simulation study. *Biophys. J.* 88:317–333, 2005.
[23]Heberle, F. A., and G. W. Feigenson. Phase Separation in Lipid Membranes. *Cold Spring Harb. Perspect. Biol.* 3:a004630, 2011.
[24]Hood, J. L., M. J. Scott, and S. A. Wickline. Maximizing exosome colloidal stability following electroporation. *Anal. Biochem.* 448:41–49, 2014.
[25]Imam, Z. I., L. E. Kenyon, A. Carrillo, I. Espinoza, F. Nagib, and J. C. Stachowiak. Steric pressure among membrane-bound polymers opposes lipid phase separation. *Langmuir* 32:3774–3784, 2016.
[26]Immordino, M. L., F. Dosio, and L. Cattel. Stealth liposomes: review of the basic science, rationale, and clinical applications, existing and potential. *Int. J. Nanomed.* 1:297–315, 2006.
[27]Kim, S. K., M. B. Foote, and L. Huang. The targeted intracellular delivery of cytochrome C protein to tumors using lipid-apolipoprotein nanoparticles. *Biomaterials* 33:3959–3966, 2012.
[28]King, J. E., E. A. Eugenin, C. M. Buckner, and J. W. Berman. HIV tat and neurotoxicity. *Microbes Infect.* 8:1347–1357, 2006.
[29]Lechardeur, D., K. J. Sohn, M. Haardt, P. B. Joshi, M. Monck, R. W. Graham, B. Beatty, J. Squire, H. O'Brodovich, and G. L. Lukacs. Metabolic instability of plasmid DNA in the cytosol: a potential barrier to gene transfer. *Gene Ther.* 6:482–497, 1999.
[30]Lee, H., J. H. Jeong, and T. G. Park. PEG grafted polylysine with fusogenic peptide for gene delivery: high transfection efficiency with low cytotoxicity. *J. Controll. Release* 79:283–291, 2002.
[31]Li, W., A. Asokan, Z. Wu, T. Van Dyke, N. DiPrimio, J. S. Johnson, L. Govindaswamy, M. Agbandje-McKenna, S. Leichtle, D. E. Redmond, T. J. McCown, K. B. Petermann, N. E. Sharpless, and R. J. Samulski. Engineering and selection of shuffled AAV genomes: a new strategy for producing targeted biological nanoparticles. *Mol. Ther.* 16:1252–1260, 2008.
[32]Li, S., and N. Malmstadt. Deformation and poration of lipid bilayer membranes by cationic nanoparticles. *Soft Matter* 9:4969–4976, 2013.
[33]Mae, M., and U. Langel. Cell-penetrating peptides as vectors for peptide, protein and oligonucleotide delivery. *Curr. Opin. Pharmacol.* 6:509–514, 2006.
[34]Mansourian, M., A. Badiee, S. A. Jalali, S. Shariat, M. Yazdani, M. Amin, and M. R. Jaafari. Effective induction of anti-tumor immunity using p5 HER-2/neu derived peptide encapsulated in fusogenic DOTAP cationic liposomes co-administrated with CpG-ODN. *Immunol. Lett.* 162:87–93, 2014.
[35]Mills, J. C., N. L. Stone, and R. N. Pittman. Extranuclear apoptosis: the role of the cytoplasm in the execution phase. *J. Cell Biol.* 146:703–707, 1999.
[36]Moghimi, S. M., P. Symonds, J. C. Murray, A. C. Hunter, G. Debska, and A. Szewczyk. A two-stage poly(ethylenimine)-mediated cytotoxicity: implications for gene transfer/therapy. *Mol Ther.* 11:990–995, 2005.
[37]Momin, N., S. Lee, A. K. Gadok, D. J. Busch, G. D. Bachand, C. C. Hayden, J. C. Stachowiak, and D. Y. Sasaki. Designing lipids for selective partitioning into liquid ordered membrane domains. *Soft Matter* 11:3241–3250, 2015.
[38]Morille, M., C. Passirani, A. Vonarbourg, A. Clavreul, and J. P. Benoit. Progress in developing cationic vectors for non-viral systemic gene therapy against cancer. *Biomaterials* 29:3477–3496, 2008.
[39]Murthy, N., J. Campbell, N. Fausto, A. S. Hoffman, and P. S. Stayton. Design and synthesis of pH-responsive polymeric carriers that target uptake and enhance the intracellular delivery of oligonucleotides. *J. Controll. Release* 89:365–374, 2003.
[40]Paluch, E., C. Sykes, J. Prost, and M. Bornens. Dynamic modes of the cortical actomyosin gel during cell locomotion and division. *Trends Cell Biol.* 16:5–10, 2006.
[41]Parker, J. N., G. Y. Gillespie, C. E. Love, S. Randall, R. J. Whitley, and J. M. Markert. Engineered herpes simplex virus expressing IL-12 in the treatment of experimental murine brain tumors. *Proc. Natl. Acad. Sci. USA* 97:2208–2213, 2000.
[42]Pecheur, E. I., and D. Hoekstra. Peptide-induced fusion of liposomes. *Methods Mol. Biol.* 199:31–48, 2002.
[43]Pires, P., S. Simoes, S. Nir, R. Gaspar, N. Duzgunes, and M. C. P. de Lima. Interaction of cationic liposomes and their DNA complexes with monocytic leukemia cells. *Biochim. Biophys. Acta Biomembr.* 1418:71–84, 1999.
[44]Rawle, R. J., B. van Lengerich, M. Chung, P. M. Bendix, and S. G. Boxer. Vesicle fusion observed by content transfer across a tethered lipid bilayer. *Biophys. J.* 101:L37–L39, 2011.
[45]Regelin, A. E., S. Fankhaenel, L. Gurtesch, C. Prinz, G. von Kiedrowski, and U. Massing. Biophysical and lipofection studies of DOTAP analogs. *Biochim. Biophys. Acta Biomembr.* 1464:151–164, 2000.
[46]Rubinson, D. A., C. P. Dillon, A. V. Kwiatkowski, C. Sievers, L. L. Yang, J. Kopinja, M. D. Zhang, M. T. McManus, F. B. Gertler, M. L. Scott, and L. Van Parijs. A lentivirus-based system to functionally silence genes in primary mammalian cells, stem cells and transgenic mice by RNA interference. *Nat. Genet.* 33:401–406, 2003.
[47]Sezgin, E., H. J. Kaiser, T. Baumgart, P. Schwille, K. Simons, and I. Levental. Elucidating membrane structure and protein behavior using giant plasma membrane vesicles. *Nat Protoc.* 7:1042–1051, 2012.
[48]Skaug, M. J., M. L. Longo, and R. Faller. the impact of texas red on lipid bilayer properties. *J. Phys. Chem. B* 115:8500–8505, 2011.
[49]Sollner, T., S. W. Whitehart, M. Brunner, H. Erdjument-bromage, S. Geromanos, P. Tempst, and J. E. Rothman. Snap receptors implicated in vesicle targeting and fusion. *Nature* 362:318–324, 1993.
[50]Tu, C. Y., L. Santo, Y. Mishima, N. Raje, Z. Smilansky, and J. Zoldan. Monitoring protein synthesis in single live cancer cells. *Integr. Biol.* 8:645–653, 2016.
[51]van Dommelen, S. M., P. Vader, S. Lakhal, S. A. A. Kooijmans, W. W. van Solinge, M. J. A. Wood, and R. M. Schiffelers. Microvesicles and exosomes: opportunities for cell-derived membrane vesicles in drug delivery. *J. Controll. Release* 161:635–644, 2012.
[52]Veatch, S. L., and S. L. Keller. Separation of liquid phases in giant vesicles of ternary mixtures of phospholipids and cholesterol. *Biophys. J.* 85:3074–3083, 2003.

[53]Veatch, S. L., and S. L. Keller. Seeing spots: complex phase behavior in simple membranes. *Biochim. Biophys. Acta Mol. Cell Res.* 1746:172–185, 2005.
[54]White, S. J., S. A. Nicklin, H. Buning, M. J. Brosnan, K. Leike, E. D. Papadakis, M. Hallek, and A. H. Baker. Targeted gene delivery to vascular tissue in vivo by tropism-modified adeno-associated virus vectors. *Circulation* 109:513–519, 2004.
[55]Wieber, A., T. Selzer, and J. Kreuter. Physico-chemical characterisation of cationic DOTAP liposomes as drug delivery system for a hydrophilic decapeptide before and after freeze-drying. *Eur. J. Pharm. Biopharm.* 80:358–367, 2012.
[56]Xu, Y. H., S. W. Hui, P. Frederik, and F. C. Szoka. Physicochemical characterization and purification of cationic lipoplexes. *Biophys. J.* 77:341–353, 1999.
[57]Yamazaki, Y., M. Nango, M. Matsuura, Y. Hasegawa, M. Hasegawa, and N. Oku. Polycation liposomes, a novel nonviral gene transfer system, constructed from cetylated polyethylenimine. *Gene Ther.* 7:1148–1155, 2000.
[58]Yang, S. T., E. Zaitseva, L. V. Chernomordik, and K. Melikov. Cell-penetrating peptide induces leaky fusion of liposomes containing late endosome-specific anionic lipid. *Biophys. J.* 99:2525–2533, 2010.
[59]Young, L. S., P. F. Searle, D. Onion, and V. Mautner. Viral gene therapy strategies: from basic science to clinical application. *J. Pathol.* 208:299–318, 2006.
[60]Zhao, J., J. Wu, and S. L. Veatch. Adhesion stabilizes robust lipid heterogeneity in supercritical membranes at physiological temperature. *Biophys. J.* 104:825–834, 2013.
[61]Zhu, S. J., D. S. P. Lansakara-P, X. R. Li, and Z. R. Cui. Lysosomal delivery of a lipophilic gemcitabine prodrug using novel acid-sensitive micelles improved its antitumor activity. *Bioconjugate Chem.* 23:966–980, 2012.
[62]Zhu, S. J., M. M. Niu, H. O'Mary, and Z. R. Cui. Targeting of tumor-associated macrophages made possible by peg-sheddable, mannose-modified nanoparticles. *Mol. Pharm.* 10:3525–3530, 2013.
[63]Zhu, S. J., P. Wonganan, D. S. P. Lansakara-P, H. L. O'Mary, Y. Li, and Z. R. Cui. The effect of the acid-sensitivity of 4-(N)-stearoyl gemcitabine-loaded micelles on drug resistance caused by RRM1 overexpression. *Biomaterials* 34:2327–2339, 2013.
[64]Zimmerberg, J., and M. M. Kozlov. How proteins produce cellular membrane curvature. *Nat. Rev. Mol. Cell Biol.* 7:9–19, 2006.
[65]Zuidam, N. J., and Y. Barenholz. Electrostatic parameters of cationic liposomes commonly used for gene delivery as determined by 4-heptadecyl-7-hydroxycoumarin. *Biochim. Biophys. Acta Biomembr.* 1329:211–222, 1997.